Hittite Journal of Science and Engineering, 2022, 9 (3) 193–204
ISSN NUMBER: 2148–4171
DOI: 10.17350/HJSE19030000271

Design and Fabrication of Soft 3D Printed Sensors and Performance Analysis of the Soft Sensors in a C-leg as Sensing Element

Doğa Ozbek **Talip Batuhan Yilmaz** **Mert Ali Ihsan Kalin** **Onur Ozcan**
Bilkent University, Department of Mechanical Engineering, Ankara, Turkey

ABSTRACT

In soft robotics, a recent challenge is to decrease the number of rigid components used to create entirely soft robots. A common rigid component used in soft robots is the rigid encoder, which should be replaced with a soft counterpart if possible. In this work, we design and manufacture a soft sensor, which is embedded into a C-shaped leg of a soft, legged, miniature robot. Our main goal is to show that we can embed a soft sensor into and receive contact feedback from a soft C-shaped leg of our soft miniature quadruped. We test various sensor parameters using custom test setups to analyze the soft sensor performance. Our soft sensor design is iterated by experimentally investigating several sensor shape options. For the C-leg of the soft miniature quadruped, optimal sensor geometry and position for the sensor implementation are found from a discrete design space as the outcome of this work. We received feedback from the soft sensor and compared commercial encoder data to the soft sensor embedded C-leg data. We managed to detect the rotation speed of the C-leg with the accuracy of 87.5% on a treadmill and with the accuracy of %86.7 under free rotation of the C-leg. However, if connection loss occurs in the miniature slipring mechanism, the error percentage in estimating the rotational speed increases significantly.

Keywords:
Soft robots; Miniature robots; Legged robots; Soft sensors; Soft robot materials and design.

Article History:
Received: 2022/07/19
Accepted: 2022/09/08
Online: 2022/09/28

Correspondence to: *Onur Özcan*
Department of Mechanical Engineering,
Bilkent University, 06800 Ankara, Turkey
Tel: +90 312 290 2893
Fax: +90 312 266 4126
E-Mail:onurozcan@bilkent.edu.tr

INTRODUCTION

In miniature soft robotics, limiting the number of rigid components to provide a soft nature to the robot is one of the most important goals. Several examples exist for soft mechanisms in biology and nature [1]. The necessary inspiration for soft terrestrial robots can be obtained from biology to imitate entirely soft creatures like worms and snakes [2]. Locomotion of the snakes or worms can be replicated using simple mechanical actuation types (extension, torsion, and bending), which the snakes or worms utilize to move in their habitats [3]. Hydraulic or pneumatic actuators can provide these actuation types; thus, these actuators have a significant role in soft robotics. These actuators can also be used for gripper mechanisms since soft gripper systems' working principle is similar to the locomotion of soft worm-like robots [4]. Some of these hydraulic or pneumatic actuators utilize self-healing ability materials, which can handle damages without losing their mechanical performance. Hyperelastic behaviors should be considered for accurate mechanical characterization of this kind of actuator [5].

An alternative to hydraulic/pneumatic soft robots is the tendon-driven soft robots in the literature. The main inspiration behind this kind of robot is the biological muscles' working principle. Tendon mechanisms are an alternative way to provide actuation to soft robots and gripper mechanisms [6]. In this type of soft robot, instead of pumps or pressurized canisters, actuation is often provided by servo or stepper motors.

Using pneumatic or hydraulic actuators or tendon mechanisms hinders the possibility of miniaturization of the soft robot design since it is challenging for a miniature robot to carry all the necessary pumps, pressurized canisters, or servo motors. To overcome this problem, actuation with shape memory alloy technology can be a solution to create soft miniature robots like it is used in the Soft Electrically Actuated Quadruped, SEAQ [7]. However, generating high voltages required for shape memory alloys and increasing the shape me-

mory alloy actuators' bandwidths are other challenges that should be tackled. Unlike the pneumatic, hydraulic, or tendon-driven actuation, we preferred micro brushed DC motors as the actuators of our robots, soft quadruped (SQuad) and modular soft quadruped (M-SQuad). Our robots SQuad [8] and M-SQuad [9] can be observed in Fig. 1 and Fig. 2, respectively.

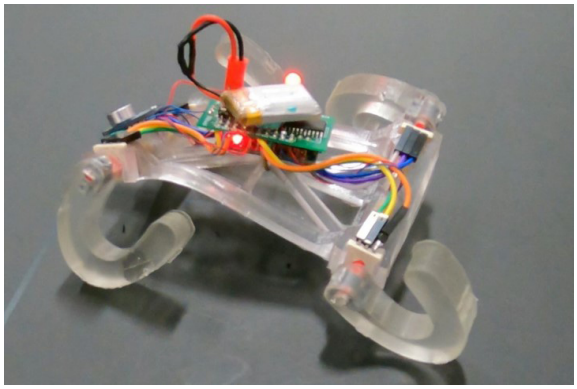

Figure 1. Miniature soft quadruped (SQuad)

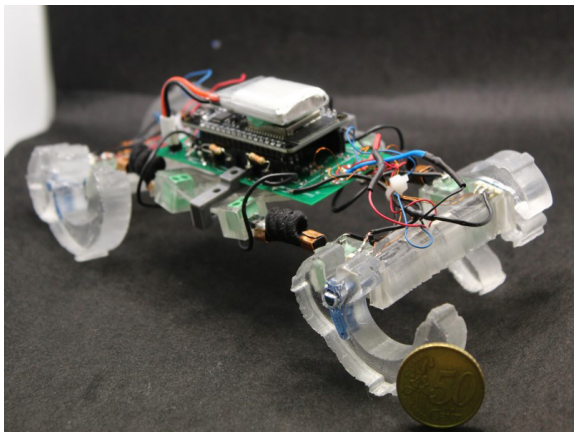

Figure 2. Modular soft quadruped (M-SQuad)

There are strategies for designing and manufacturing entirely soft robots since it is one of the trending topics in soft robotics [10]. However, the locomotion capabilities of such robots are still quite limited. To provide joint position feedback for gait control or environmental perception for decision-making, rigid sensors can be used in soft robots; however, they have the potential to ruin the soft nature of the robots [11]. Soft stretchable sensing elements are one of the trending topics for both soft robotics and wearable technologies [12]. In literature, there is a soft gripper that can detect chemicals in the environment by using engineered bacteria [13]. Soft sensors can also be implemented on the human body to assess human gait [14], [15]. Several other examples exist for soft electronic skins; however, no soft sensors are implemented on a soft miniature mobile robot until M-SQuad is developed. M-SQuad uses the soft sensors on its body to distinguish whether the obstacle it encounters is scalable. This is the main difference between SQuad and M-SQuad [8], [9]. It should be noted that none of these robots have soft sensors in their C-legs. They utilize rigid encoders to control their gaits.

The main challenge behind soft sensors on miniature soft robots is the nonlinear nature of soft sensors, as they mainly depend on resistance change. Preferring capacitive sensing to resistance-based sensing is another way to deal with the nonlinearity issue. It is even possible to create a soft accelerometer with soft conductive materials using capacitive sensing [16]. The nonlinearity directly affects the quality, reliability, and repeatability of the data acquired from soft sensors. Researchers often use machine learning models to compensate for the nonlinearity [17]. However, M-SQuad uses the raw data from the soft sensors to distinguish whether it can climb over the obstacle it encounters or not [9].

Different kinds of soft sensors exist, such as soft pneumatic sensing chambers. However, to acquire and record the response of these kinds of sensors, often sophisticated electronics are needed [18]. Since it is not easy for a soft miniature mobile robot to carry large and sophisticated electronics during its locomotion, such a sensor is unsuitable for our case. Furthermore, there are also highly stretchable optical sensors for detecting pressure, strain, and deflection. These kinds of sensors have accurate and high-precision responses [19]. However, the design and manufacturing of these sensors are complicated and require significant expertise in optics.

In this study, we aim to assess the feasibility of implementing soft sensor technology into the C-legs of SQuad. The motivation behind this idea is to evaluate the terrain information and replace hard commercial encoders with soft sensors by embedding soft sensors into the C-legs. Two experimental test setups are developed to assess this idea's feasibility. In the axial loading test setup, a soft sensor embedded C-leg can be compressed axially by controlling the compression speed and the amount of compression. In the treadmill test setup, C-leg is inserted into a tower with a miniature slipring specially designed to acquire data from the rotating C-leg. Sensorized C-leg is simulated in robots' locomotion in this test setup. Sensor responses are acquired in both test setups. Additionally, encoder data is also obtained in the treadmill test setup.

The main contributions of this work are the design of sensorized C-legs, the design of a miniaturized slipring to receive sensor data, and the determination of the optimal sensor geometry and the optimal position for the sensor implementation, both within a discrete design space, by assessing the experimental data obtained from both test setups.

PROBLEM STATEMENT

On SQuad, infinite-turn potentiometers are used as encoders to obtain angular position feedback from the motors. However, the encoders are entirely rigid components. To improve the compliance of the robot, soft sensor embedded C-legs may replace these rigid encoders. At the very least, the soft sensor embedded C-legs have the potential to acquire terrain information, such as assessing the hardness or roughness of the terrain.

To assess the feasibility of this concept, the starting point is the analysis of the mechanical properties of the regular C-leg and the soft sensor embedded C-leg. Since the regular C-leg is known to work quite successfully in SQuad, we would like the composite C-leg to have similar mechanical properties. Composite mechanics theories are used to assess the mechanical properties of the soft sensor embedded C-leg. After mechanical properties analysis of the composite C-leg, stiffness analysis is conducted using the Finite Element Method (FEM) experimental results.

Another critical challenge in utilizing the soft sensors in our soft robot's legs is the electrical connection from a constantly rotating structure to a fixed electrical board. The electrical connection should be provided from the C-legs to the microprocessor during a full rotation of the C-leg. For this purpose, a miniature slipring mechanism is specially designed and manufactured. It has a significant role in electrical connections for soft sensors. Without this mechanism, there is no way to implement soft sensors in the robot to replace the encoders.

Moreover, the performance of the sensorized C-legs needs to be examined before it is integrated into the soft miniature robot. For this purpose, a test setup is specially designed. In this setup, C-leg is attached to the same micro brushed DC motor via the miniature slipring and is rotated. Soft sensor and encoder responses are recorded simultaneously while the leg runs on a treadmill. By using the results of this experiment, the performance of the sensorized C-leg and the reliability of the designed miniature slipring can be simulated.

Last but not least, optimal sensor geometry and position should be determined for using the soft sensors on the soft miniature robot. The choice of sensor geometry and the position is a continuous parameter and therefore has an infinite number of potential values. Thus, the selection is made using a discrete design space after ensuring that the composite leg's material properties are similar to the regular leg and that the electrical connection between the sensorized leg and the microcontroller is reliable. The experiments explained in the following section are designed to decide the optimal sensor geometry and position.

OUR SOLUTION: SENSORIZED LEG

Soft Sensor

In this work, we design soft sensors that change their electrical resistance values when they experience mechanical inputs, i.e., soft strain gages. To assess the different soft sensor geometry options, nine different sensor geometries are designed by preserving the dimensions of 26 mm x 9 mm x 1 mm for each geometry, as it is shown in Fig. 3. SQuad's C-legs have the dimensions of 36 mm, 40 mm, and 10 mm, in lateral, longitudinal, and thickness directions. We planned to place eight sensors in a leg for the experiments, as shown in Fig. 4(b). To fit the eight sensors in the C-legs in the configuration shown in Fig. 4(b), the dimensions of sensor geometries are set to 26 mm x 9 mm x 1 mm. Selecting the dimensions any bigger causes contact between sensors for these experiments. The sensor geometries are designed with inspiration from basic geometric features like triangles, squares, hexagons, zigzag lines, etc. There is an infinite number of geometries for the soft sensors. Since we cannot assess an infinite number of geometries, we discretized the number of sensor geometries that will be investigated. We have selected the sensor geometries by considering the various amount of strain each sensor geometry encounters. We cannot guarantee that the best geometry among our trials is the optimum sensor geometry; there can be sensor geometries we could not think of and did not try that may bring better results. The black parts of the designs show the conductive regions, whereas the gray part shows the non-conductive regions of the soft sensors. The conductive parts of the sensors are 3D printed from conductive Thermoplastic Polyurethane (cTPU).

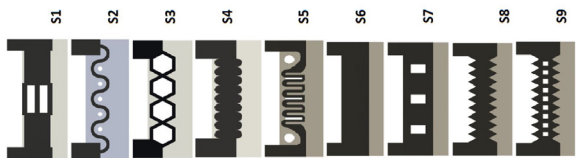

Figure 3. Nine different sensor geometries with the dimension of 26 mm x 9 mm x 1 mm

(a) (b)

Figure 4. (a) Soft sensor embedded C-leg (Composite C-leg) and (b) its sensor placed mold

During 3D printing, the number of wall perimeter layers is set to one except for the top and the bottom layer wall perimeters, which are set to three. Furthermore, the first layer height is set at 0.27 mm, whereas the other layer heights are kept at 0.18 mm. Thus, there was no need to select the infill rate since the sensors are designed with 1 mm thickness. Nozzle temperature is set to 230°C, and the heat bed temperature is set to 65°C. A second extruder combines cTPU and regular, non-conductive Thermoplastic Polyurethane (TPU) to manufacture the sensor geometries.

Soft Sensor

The dimensions of the C-leg in the lateral direction, longitudinal direction, and thickness are 36 mm, 40 mm, and 10 mm, respectively. Longitudinal direction represents the direction of gravity, whereas lateral direction represents the SQuad's moving direction during locomotion. C-legs are manufactured with almost the same technique used in manufacturing SQuad's C-legs. Since the primary material is PDMS, the molding technique is utilized. Molds are 3D printed using 3D printer filament, Polylactic Acid (PLA). Then, PDMS Sylgard 184 was mixed in a 5:1 ratio of a pre-polymer and cross-linker, and the mixture was poured into the mold. To embed the 3D-printed soft sensors, channels are created in the mold to place the soft sensors before pouring PDMS into the mold. The number and position of the soft sensor channels differ in the molds according to the experiments. In this study, we aim to assess the optimal position for the soft sensor placement in the C-leg and the effect of the embedded sensor on the longitudinal stiffness of the C-leg. Thus, we designed two different types of C-leg molds. One mold contains a single channel, as shown in Fig. 4a. In contrast, the other mold has additional two channels with an equal distance of 1.5 mm to the channel located in the middle of the mold, as shown in Fig. 5a. The second mold enables us to place eight soft sensors in a single leg at different positions within the leg. The channel width and length were kept the same for both designs as 1 mm and 50 mm, respectively. Molds of the soft sensor embedded C-legs (composite C-legs) can be observed in Fig. 4a, and the manufactured composite C-legs can be observed in Fig. 4b. The mold of eight soft sensors embedded C-leg can be observed in Fig. 5a and the manufactured multisensory embedded C-leg is shown in Fig 5b.

Slipring Mechanism

An electrical connection mechanism is designed to receive a continuous electrical reading from the embedded soft sensor located at the rotating C-leg. The working principle of this mechanism is somewhat similar to a commercial pancake-type slipring. However, a few miniature pancake-type sliprings have an outer diameter of less than 8 mm on the market. The mechanism can be

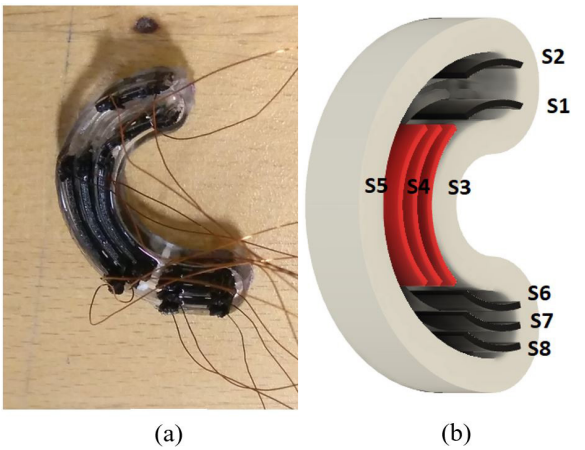

Figure 5. (a) Eight-sensor-embedded C-leg and (b) its mold

observed in Fig. 6. Design mainly consists of two hollow tubes and two bearings next to each other. Each hollow tube mechanically connects to one of the bearings. The long and smaller diameter hollow tube connects the motor to the leg. The outsides of the bearings do not rotate with the leg and are used for electrical connections. A polyimide film is placed between the two hollow tubes to isolate the tubes and the sensor connections electrically. The bearings provide the bedding for the rotating shaft in the treadmill test setup. They are also pinouts where the cables from the DAQ are soldered to.

Figure 6. An assembled version of the slipring mechanism and its CAD drawing.

METHODS

Evaluation of Soft Sensor Embedded C-leg's Mechanical properties

We would like to acquire a sensorized C-leg with similar mechanical properties (Young's modulus, Poisson's ratio, shear modulus, etc.) to a regular, molded from pure PDMS C-leg because we have shown PDMS legs to function very well in our previous works. Since a 3D printed soft sensor is embedded into a C-leg mainly consisting of PDMS, the resulting structure can be evaluated as a composite material. PDMS part of the C-leg can be considered the composite matrix, where the embedded sensor is the composite fiber. C-leg has a continuous volume along its C shape. There are unit volumes sampled from the upper end, middle, and bottom end of the C-leg, and each has respective directions, as shown in Fig. 7. The orientation of both the transverse direction and the longitudinal direction changes along the continuous C Shape volume of the leg. For instance, both transverse and longitudinal directions are in the same orientation as the transverse direction and the longitudinal direction of the C-leg,

where the bottom end and upper end are opposite to the transverse direction and the longitudinal direction of the C-leg. The composite material properties are calculated by considering the unit cubic volumes sampled from the continuous C shape volume of the leg. A schematic of the composite material and the unit volume valid for calculations are shown in Fig. 7.

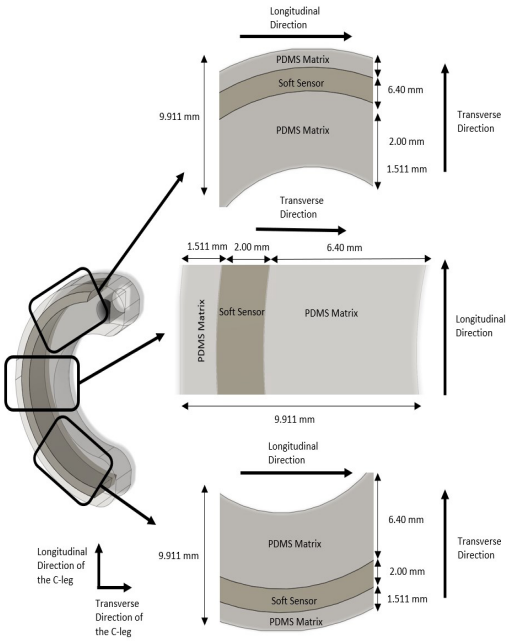

Figure 7. A schematic of the composite material and the unit volume valid for calculations

Since sensor embedded C-leg is considered composite, the following composite mechanics theories can be applied:

$$f = \frac{t_f}{t_f + t_m} \tag{1}$$

where t_f is the thickness of the fiber, t_m is the thickness of the matrix, and f is the fiber volume ratio.

$$E_1 = f\,E_f + \left[1 - f\right]E_m \tag{2}$$

$$E_2 = \frac{E_f E_m}{f\,E_m + \left[1 - f\right]E_f} \tag{3}$$

where E_f is the Young's Modulus of the fiber, E_m is the Young's Modulus of the matrix, E_1 is the Longitudinal Young's Modulus, and E_2 is the Transverse Young's Modulus.

$$v_{12} = f v_f + \left(1 - f\right)v_m \tag{4}$$

where v_f is the Poisson's Ratio of the fiber, v_m is the Poisson's Ratio of the matrix, and v_{12} is the Major Poisson's Ratio.

$$\frac{1}{\mu_{12}} = \frac{f}{\mu_f} + \frac{1 - f}{\mu_m} \tag{4}$$

where μ_f is the Shear Modulus of the fiber, μ_m is the Shear Modulus of the matrix, and μ_{12} is the Shear Modulus of the composite.

$$\sigma_{ys_c} = f\,\sigma_{ys\,f} + \left[1 - f\right]\sigma_{ys_m} \tag{6}$$

where σ_{ys_f} is the Yield Strength of the fiber, σ_{ys_m} is the Yield Strength of the matrix, and σ_{ys_c} is the Yield Strength of the composite.

$$\sigma_{ts_c} = f\,\sigma_{ts\,f} + \left[1 - f\right]\sigma_{ts_m} \tag{7}$$

where σ_{ts_f} is the Tensile Strength of the fiber, σ_{ts_m} is the Tensile Strength of the matrix and σ_{ts_c} is the Tensile Strength of the composite.

$$\rho_c = f\,\rho_f + \left[1 - f\right]\rho_m \tag{8}$$

where $\tilde{n}_f$ is the density of the fiber, $\tilde{n}_m$ is the density of the matrix, and $\tilde{n}_c$ is the density of the composite [20].

Using Eq. (1) to Eq. (8), the mechanical properties of the composite C-leg are calculated, and the results are further discussed in the results and discussion section.

Finite Element Analysis to Determine the Stiffness of the C-legs

Finite Element Analysis (FEA) is conducted to evaluate the stiffness values of the soft sensor embedded C-leg and the regular C-leg (without the soft sensors) in the simulation environment. The linear elastic material assumption is used for all structural analyses. The magnitude of the force applied for both the regular C-leg and the soft sensor embedded composite C-leg is set to 1 N. As the boundary conditions of FEA, fixed surfaces are selected as the bottom surface of the C-leg. An automatic contact tool is used to preserve the composite structure of the soft sensor embedded C-leg. Embedded sensors are considered fibers, whereas the PDMS is regarded as the matrix for the composite C-leg. The tolerance for the automatic contact tool is set to 0.01 mm.

Experiments to Evaluate the Stiffness of Soft Sensor Embedded C-leg

Experiments to evaluate the stiffness of the soft sensor embedded C-leg is conducted using a custom-made compression test setup. In this experiment, the regular C-leg and the soft sensor embedded C-leg are placed into the test setup. The C-leg's bottom end is attached to the fixed bottom end of the compression test setup, where a force sensor is located. The amount of comp-

ression is set to 12 mm for both the soft sensor embedded C-leg and the regular C-leg, where the compression rate is set to 0.8 mm/s. The 12-mm-compression amount is almost four times the actual displacement amount that occurs during robot locomotion. Compression occurs in only the longitudinal direction of the C-leg up to 12 mm; hence this compression amount is chosen. Compression speed is preferred as the slowest speed possible since we want to make qualitative and quantitative observations. The setup provides force versus displacement data for the C-leg attached. The data gathered is post-processed using MATLAB to find the stiffness of the attached C-leg along the longitudinal direction. The test setup can be observed in Fig.8.

In the compression tests, the main goal is to investigate the change in the stiffness of the leg in the longitudinal direction when the sensors are embedded. We hypothesized that embedding a soft sensor into a C-leg will create a composite structure for the C-leg; thus, the stiffness of the C-leg will change. However, if the stiffness change is not significant, this change would not affect the locomotion much and would be acceptable.

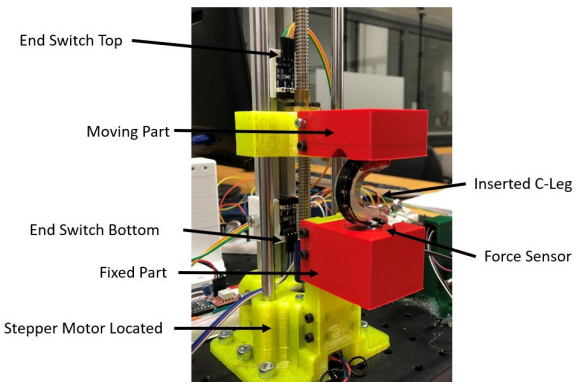

Figure 8. Axial compression test setup for the C-leg stiffness analysis experiments

Experiments to Assess the Soft Sensor Performance

Experiments to assess the soft sensor performance is conducted using the treadmill test setup. In this setup, C-legs are simulated as they are attached to SQuad's body during locomotion. By rotating the C-legs freely at 0.3 Hz in air, with no treadmill contact, a baseline for the embedded soft sensor detecting the inertial effects of a freely rotating C-leg is established. C-legs are also rotated on the treadmill test setup to observe how the sensor would behave during the locomotion of SQuad. Both cases' sensor response is captured via the slipring mechanism developed and the DAQ system.

The treadmill test setup is designed to simulate the C-leg behavior during SQuad's locomotion on the ground. It consists of two towers and one treadmill. The encoder, which is used to have angular position feedback and angular speed feedback from the C-leg, is placed into one tower. The slipring mechanism, designed to acquire soft sensor response from rotating C-legs, is positioned in the other tower. These two towers are connected via an extended camshaft that also carries the rotating C-leg. C-leg runs on the treadmill, which imitates the ground contact of the C-leg while the SQuad is walking. Because the SQuad body's vertical position changes during locomotion, the treadmill is fixed to the setup through four soft springs, one for each corner, which acts as a soft suspension for the ground. Using this suspension system, the motor's relative distance to the ground can change. Users can input the angular speed of the rotating C-leg and the initial height of the treadmill and record soft sensor response and the encoder data simultaneously via the data acquisition system. CAD drawing of the treadmill test setup and its fully assembled version can be seen in Fig. 9.

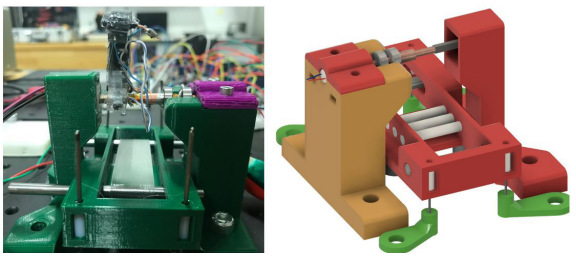

Figure 8. Fully assembled version of the treadmill test setup and its CAD drawing

Experiments to Find the Optimal Sensor Geometry in the Discrete Design Space

The compression setup has two fixed ends and a moving module where the C-legs can be attached. Motion is controlled by stepper motors located at the bottom of the compression test setup. An aluminum beam is integrated into the design to carry the statical load of the assembled test setup. The rest of the parts are 3D printed. There are also aluminum rods with 8-mm-diameter to provide alignment and guidance. Linear bearings provide a smooth motion for the moving module. Two limit switches are added for both safety and calibration. The user inputs a compression amount and compression speed to the microcontroller, and the setup compresses the C-leg in the longitudinal direction until the input compression is reached. It waits for one second and then decompresses the C-leg to the initial position. Users can record the instantaneous sensor response respective to the time as the experiment outcome from this setup. CAD drawing of the compression test setup can be seen in Fig. 10.

Homogenous and periodic compression can be applied on different soft sensors by controlling compression amount and compression speed in the axial compression test

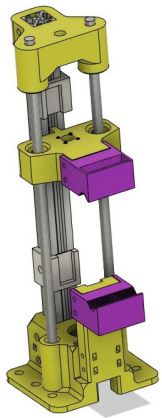

Figure 10.CAD drawing of the axial compression test setup

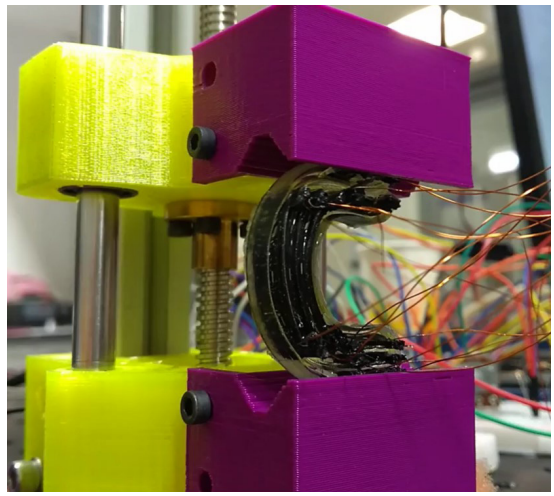

Figure 11. Compression of eight-sensor-embedded C-leg in the axial compression test setup.

setup. In this study, the angle of contact between the C-leg and the ground is set to 90 degrees in all experiments, which means the contact point is farthest away from the motor mount during the experiments. With the axial compression test setup, experiments are conducted to find the optimal sensor geometry among the nine different geometries previously listed for the sensor-embedded C-leg. For this purpose, nine different sensor geometry was designed by keeping the dimensions 26 mm x 9 mm x 1 mm for each sensor geometry. 6 mm compression, almost two times the leg's actual displacement during the robot's locomotion, was applied to each soft sensor geometry. Compression speed and release speed were set to 3 mm/s, meaning the duration for both compression and release is 2 seconds. Each cycle consists of compression of the C-leg, waiting for a one-second delay, and then release of the C-leg. Therefore, cycle time becomes 5 seconds, which is slow enough to make qualitative and quantitative observations. Each experiment consists of 4 cycles. As the experiment result, sensor response in voltage versus elapsed time was gathered from the DAQ system.

Experiments to Find the Optimal Sensor Position out of Eight Positions Defined in the C-leg

Experiments to find the optimal position for a soft sensor in the C-leg were conducted using the axial compression test setup shown in Fig. 10. In these experiments, eight identical sensors are embedded into a soft C-leg attached to the moving module of the axial compression test setup. Each of the sensors was embedded into different locations in the soft C-leg. Most experiment parameters (compression speed, release speed, content of one cycle) were kept the same as the experiments conducted to find the optimal sensor geometry. As the experiment outcome, the sensor response of all eight sensors in voltage respective to the elapsed time was gathered simultaneously from the DAQ system. A snapshot from one of the sensor position experiments is shown in Fig. 11.

Electronics

Data Acquisition System (DAQ) has a significant role in electronics design. A typical Wheatstone bridge architecture is used to transform the resistance change of the sensor into a voltage signal. As in standard Wheatstone bridges, one arm of the bridge is formed by the sensor, whereas the rest of the arms are formed by fixed resistances. Wheatstone bridges are built by considering the nominal resistances of the soft sensors, i.e., unloaded sensor resistances. A soft sensor is placed as one of Wheatstone's four resistances, whereas the other three fixed resistances of the bridge are selected close to the nominal sensor resistance to get the output with the maximum range from the Wheatstone bridge. The outputs of the Wheatstone bridges are directly connected to the DAQ, which has eight input channels that can receive signals simultaneously. In the compression test setup, a microprocessor (Arduino Pro Micro) is used to receive and execute commands from the user. A stepper motor driver drives the Stepper motor with the digital signals from the microprocessor. In the treadmill test setup, the response of the sensorized C-leg is recorded with the same Wheatstone configuration and a DAQ channel, and another channel of DAQ is used to record the encoder data when the C-leg is rotating in the test setup. A 700:1 gear ratioed micro brush DC motor, the same motor used on SQuad, rotates the C-leg in the test setup. The frequency of the rotation is controlled by a microprocessor (Arduino Pro Micro).

RESULTS AND DISCUSSION

Evaluation of Soft Sensor Embedded C-leg's Mechanical properties

Evaluation of composite and regular soft C-leg material properties is made using Eq. (1) to Eq. (8) in the methods section. The fiber volume ratio is calculated using the CAD drawing of the soft sensor embedded C-leg to conduct the calculations. Table 1 includes the mechanical properties of TPU, PDMS, and created composite ma-

terial. Continuous C shape volume is discretized for the composite mechanics calculations by sampling the unit cubic volumes from the C-leg. It was shown that Young's modulus of the C-leg becomes almost four times.

Stiffness analysis experiments and FEA are conducted to assess the stiffness change along the longitudinal direction of the C-leg. Yet, because PDMS is already a pretty soft material (in the low few MPa range), the resulting material is still in the same few MPa range and could be assumed soft. Therefore, the change in Young's Modulus and the consequent change in stiffness is expected not to change the locomotion properties much because the order of magnitude of the Young's Modulus and the stiffness remains the same.

Table 1. Calculated composite material properties by using Eq. (1) to Eq. (8)

Parameters	*TPU (Fiber)*	*PDMS (Matrix)*	*Composite*
σ_{ys}	*7.6 MPa*	*15 MPa*	*13.52 MPa*
σ_{ts}	*30 MPa*	*12 MPa*	*15.60 MPa*
ρ	*1.248 g/cm³*	*0.97 g/cm³*	*1.03 g/cm³*
ν	*0.39*	*0.49*	*0.47*
μ	*58.7 MPa*	*0.6 MPa*	*0.74 MPa*
E_{Lf}	*0.023 GPa*	*0.0015 GPa*	*0.0058 GPa*
E_{Tf}	*0.023 GPa*	*0.0015 GPa*	*0.0019 GPa*

Finite Element Analysis to Determine the Stiffness of the C-legs

In this analysis, 1 N is applied in the y-direction for both cases. Distributed displacement along the longitudinal direction on both the regular C-leg and composite C-leg can be observed in Fig. 12 and Fig. 13, respectively. Maximum absolute displacement along the longitudinal axis is found as 5.49 mm for the regular C-leg, whereas it is found as 2.95 mm for the composite C-leg. Since the compression amount and applied force are known, it is possible to apply Hooke's law to determine the stiffness of each C-leg. For the regular C-leg, stiffness is found as 182.15 N/m, whereas it is found as 338.87 N/m for the composite C-leg. Embedding the soft sensor into C-leg increased the stiffness to almost twice, by 85.6%.

The longitudinal Young's modulus of the composite material was calculated as 5.8 MPa, whereas Young's modulus of the PDMS was known as 1.5 MPa. However, the change in leg stiffness is only found to be from 338.87 N/m to 182.15 N/m. The main reason for this discrepancy is that composite mechanics calculation considers unit volumes sampled from the C-leg's upper, middle, and bottom end. From the upper end to the bottom end, the longitudinal and transverse directions of the sampled unit volume do not match C-leg's longitudinal and transverse directions. Therefore, it is impossible to evaluate the change in leg stiffness respective to the longitudinal Young's modulus of the composite material in this case. These composite mechanics calculations are made for approximating the mechanical properties of the composite material created with PDMS and cTPU sensor.

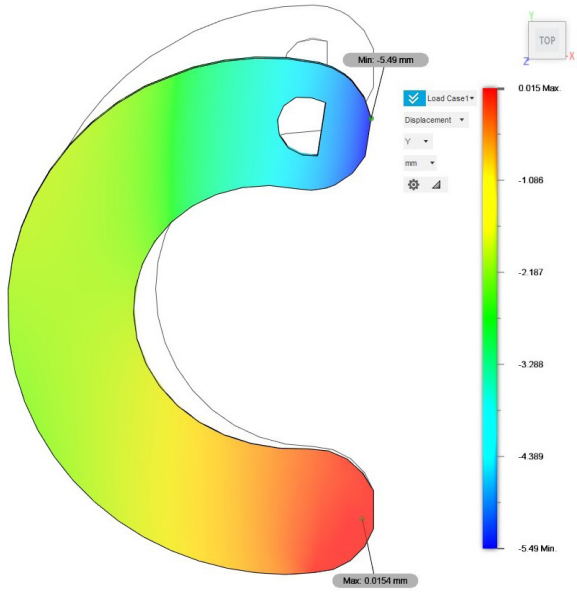

Figure 12. Structural analysis of the regular C-leg: blue color indicates the negative displacement, whereas the red color indicates the positive displacement. The compression applied is in the negative Y direction with respect to the coordinate supplied in the figure. All the displacements are in mm.

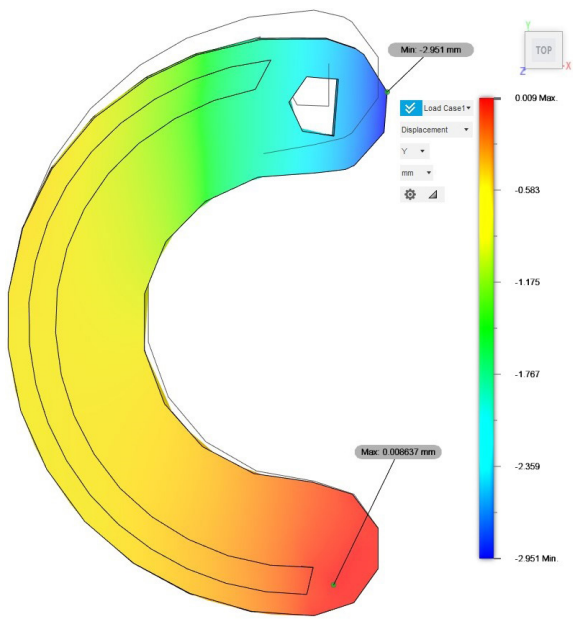

Figure 13. Structural analysis of the composite C-leg: blue color indicates the negative displacement, where red color indicates the positive displacement. The compression applied is in the negative Y direction with respect to the coordinate supplied in the figure. All the displace-

Experiments to Evaluate the Stiffness of Soft Sensor Embedded C-leg

This experiment gathers compression amount versus applied force data for both the regular C-leg and the soft sensor embedded C-leg. Data is represented in Fig. 14 and Fig. 15, respectively. The experimental stiffness of both legs can be found by finding the slope of these two plots. The results of this experiment are compared to the FEA conducted before. The outcome of this comparison can be observed in Table 2.

Table 2. Comparison of stiffness experiment results and FEA results.

Leg Type	*Stiffness from FEM*	*Stiffness from Experiments*	*Error (%)*
The regular C-Leg	*182.15 N/m*	*229.72 N/m*	*20.7%*
Composite C-Leg	*338.87 N/m*	*295.90 N/m*	*12.7%*

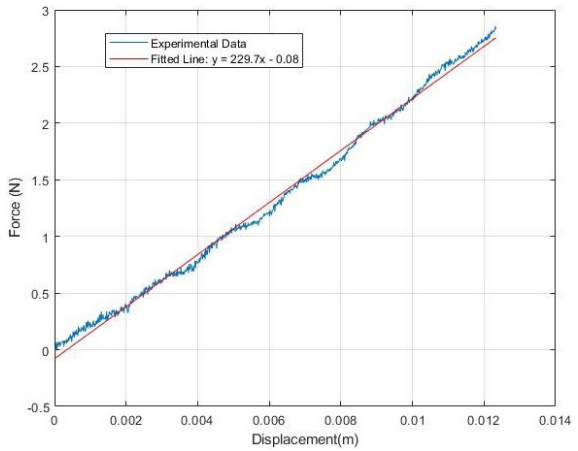

Figure 14. Force versus displacement for casual C-leg

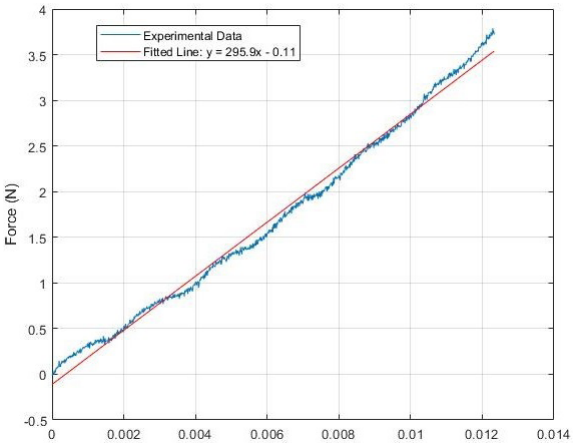

Figure 15. Force versus displacement for composite C-leg

Stiffness values are found by using FEM and conducting experiments. Percentage errors are calculated for both legs. Minor manufacturing errors, the D shaft housings located in the PDMS matrix for connection purposes, or even a slight mismatch between the reported Young's Moduli of the materials used and their actual values can account for the slight mismatch between the FEA results and the experimental findings. Either case, the composite nature of the sensorized C-legs does not change the stiffness value of the legs in an amount that would significantly alter locomotion characteristics, i.e., the legs are still expected to deflect a significant amount during locomotion and cause the robot to walk like a soft robot, rather than a rigid one.

Experiments to Evaluate the Fatigue Life of Soft Sensor Embedded C-leg

In this experiment, a soft sensor embedded C-leg is attached to the treadmill test setup, as shown in Fig. 9. It is rotated at 1 Hz for a full day to check whether it survives without any damage. It survived without any damage, which means it handled almost 86400 cycles. After all structural experiments, even now, it is still available to use. Compared to other components of the SQuad, the cycle life of the soft sensor is far better.

Experiments to Assess the Soft Sensor Performance

In this experiment, we aim to compare the soft sensor performance to the commercial encoder currently used on SQuad. C-leg is attached to the treadmill test setup and rotated at 1 Hz for 30 seconds. Free rotation and rotation on treadmill cases are investigated. Three clear peaks of triangular-shaped commercial encoder signal can be observed in Fig. 16 and Fig. 17 for both cases. Three respective responses can be observed in the soft sensor responses for both cases. A promising observation of the experiment was that the soft sensors even captured the inertial forces due to the rotation of the C-leg, as shown in Fig. 16. When the C-leg is placed onto the treadmill, the amplitude of the soft sensor response increases since the cyclic load applied from the ground is increased as can be observed from Fig. 17.

The soft sensor response's peak amplitude is much smaller than the encoder response. Despite this, the soft sensors seem to be following a trend that could be correlated with the stepping pattern. On the other hand, the sensor response cannot be used to distinguish the C-leg's angular position without any postprocessing such as filtering, fitting a function, or potentially some machine learning methods. Instantaneous, non-delayed angular position and rotational speed information are needed to control the robot's gait. Thus, even if a simple moving average filter is applied to the robot, the gait control of the robot may be broken due to the time delay introduced by the filter. We only eliminate the dead zone for the commercial encoder by simple thresholding without introducing time delay. At this point, acquiring instantaneous angular position information does not seem possible with the current soft sensor response. Hence the sensor is not applicable for gait control under the current control scheme.

However, it is possible to capture the rotational speed of the leg with these soft sensors in both free rotation and on treadmill cases. In the first three seconds, three repeating patterns were expected to be observed in the soft sensor response since the rotation speed of the C-leg was set to 1 Hz. In both Fig. 16 and Fig. 17, three repeating patterns exist in the first three seconds of the experiment. We constructed an algorithm that counts how many times soft sensor responses reach or pass a defined threshold. A timer is also used to capture the elapsed time during the counting process. For instance, the threshold is set to be between -0.2 V and -0.15 V for free rotation, whereas it is set to be between 0.45 V and 0.46 V for the treadmill case. For the commercial encoder, the threshold is set to be between -0.55 V and -0.45. The counter is divided into four because we observed in each pattern that soft sensor response creates an "m shape," meaning almost two symmetrical peaks exist.

On the other hand, to estimate the rotation speed with commercial encoders, the counter is divided into two since each pattern consists of a single peak. After the division, we have the number of revolutions and time elapsed. By using these two features, the rotational speed can be calculated respectively.

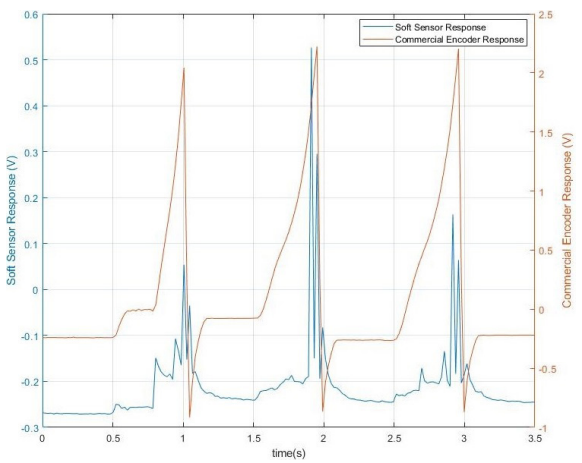

Figure 16. Soft sensor and commercial encoder responses under free rotation

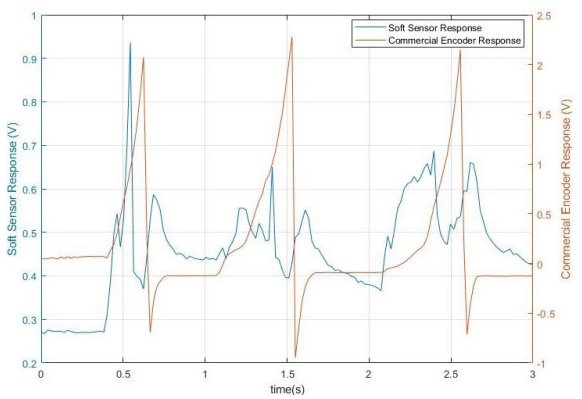

Figure 17. Soft sensor and commercial encoder responses on the treadmill

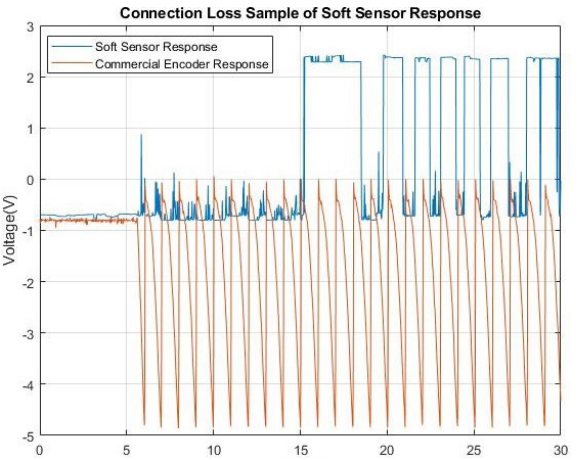

Figure 18. Connection loss sample of soft sensor response

Furthermore, one of the significant observations was the connection loss due to slipring reliability issues. Although it rarely happened, it affected the results of some experiments, as shown in Fig. 18. Connection loss directly affects the error percentage in estimating the rotational speed of the C-leg. Once a connectivity issue occurs in the slipring mechanism, it continues to affect the sensor response unless it is manually fixed, as can be observed in Fig. 18. If there are no connectivity issues in the slipring mechanism, we found that the algorithm can detect the rotational speed with an accuracy of 86.7% for the free rotation case. Moreover, the accuracy of detecting the rotational speed is 87.5% for the treadmill case. We cannot claim any accuracy on the rotational speed estimation when a connectivity issue occurs because estimating rotational speed is almost impossible before manually fixing the connectivity issue.

Experiments to Find the Optimal Sensor Geometry

In this experiment, nine sensors with the same dimensions are compressed in the axial compression test setup by keeping compression speed and amount fixed. Each sensor response can be observed in Fig. 19. Sensors 1-6 and 8 have peak-to-peak amplitudes less than 10 mV, whereas sensors 5, 7, and 9 have peak-to-peak amplitudes higher than 15 mV. Therefore, by investigating the amplitude of the responses, sensors 5, 7, and 9 are selected due to their relatively large amplitudes. The same response trend (the "m" shape) is observed for all sensors. At each cycle, a waiting period of one second is observed between two peaks of m shape. To select the optimal geometry, the clarity of detecting the waiting period in a cycle was chosen as the criterion because, for an angular position determination algorithm, this would give the most significant number of features. By considering this criterion, sensor 7 is selected to continue with.

Experiments to Find the Optimal Sensor Position

It is possible to place only eight sensors in a C-leg without

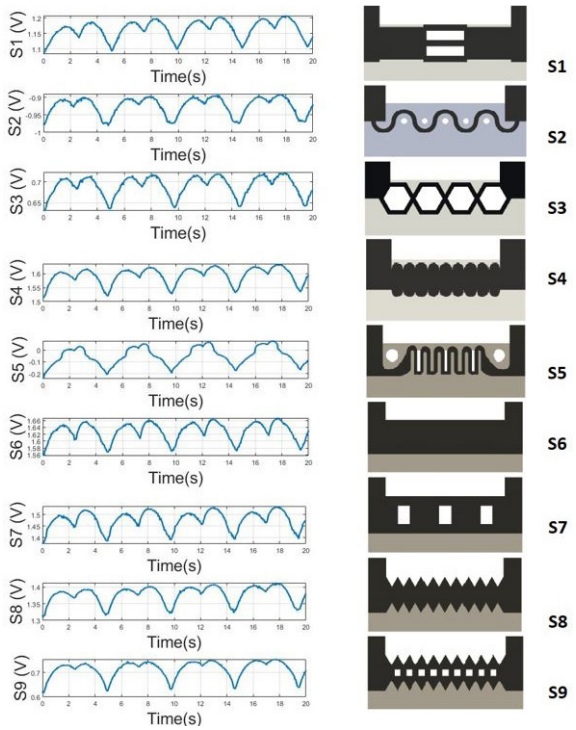

Figure 19. Responses of nine sensors with different geometries versus time

causing significant cracks. Sensors are labeled as shown in Fig. 5a. Each soft sensor response inside the C-leg can be observed in Fig. 20. To assess the optimal sensor position, the clarity of detecting the sensor response regime and peak-to-peak amplitude of the soft sensor response was set as the criteria. Considering these criteria, the performance of sensors located at both the top and bottom ends of C-legs was better. Sensors located in the middle of the C-leg were not significantly affected. This was expected since we had observed upper ends of the C-legs deflect the most in FEA analysis of the C-legs. The bottom ends of C-legs were not affected that much since it is assumed as the fixed end in structural analysis. At the end of this experiment, although it is observed that both the bottom and upper ends of C-legs are affected by the compression, we preferred a longer and continuous sensor along the channel located in the middle since the peak-to-peak amplitude is much higher for sensors located at the center. Furthermore, increasing the length of the sensor will provide more mechanical deflection for the sensor. Thus, it will provide a sensor response with a higher peak-to-peak amplitude.

CONCLUSION

This study aimed to assess the possibility of replacing the commercial encoders with soft sensors embedded into the C-legs of the SQuad. Optimal sensor geometry is determined by experiments on the axial compression test setup. The optimal position to place the soft sensor is

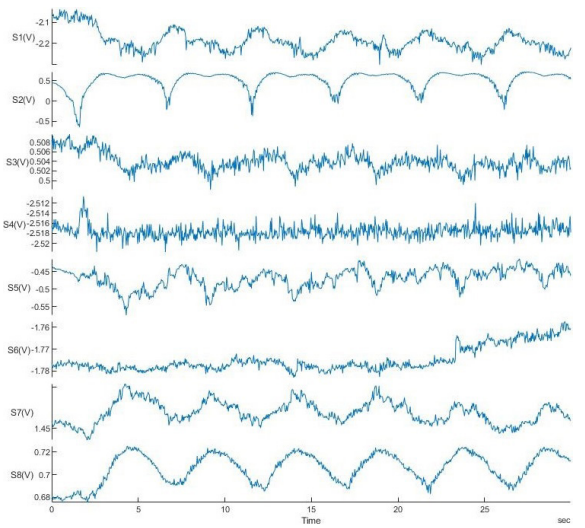

Figure 20. Response of eight soft sensors embedded into the C-leg respective to the elapsed time

also found using experiments done on the axial compression test setup. The stiffness values of the legs are analyzed with FEA conducted on both the regular C-leg and composite C-leg. Stiffness change is calculated from the outcome of the FEA; however, stiffness experiments are conducted on both legs to verify this FEA outcome. In addition, the response of the soft sensor embedded into the C-leg is compared with the commercial encoder used on the robot to assess the soft sensor's performance. After various experiments conducted on soft sensor embedded C-leg, it is observed that embedding a soft sensor into the C-leg changes the mechanical properties of the C-leg. Although embedding a soft sensor changes the mechanical properties of the C-leg, it allows us to estimate the rotational speed of the C-leg for both the treadmill and the free rotation cases with an accuracy of 87.5% and %86.7, respectively.

On the other hand, connection loss may occur during gathering data from the soft sensor embedded into C-leg. This can happen because of reliability issues of the slipring mechanism and the sensor misalignments that occurred inside the C-leg. The amount of error can increase depending on the duration of the connection loss. Thus, this risk should always be considered for the calculations.

In future work, we plan to integrate this slipring mechanism into the SQuad. We want to investigate the sensor's performance on the complete robot. This will give us a more accurate idea about the feasibility of replacing commercial encoders with soft sensors we developed. These sensors will gather information about terrains, such as the terrain material or the terrain roughness. As the first step for this, using the treadmill test setup, C-leg can be simulated on different terrains such as sand, glass, rubber, or metal.

CONFLICT OF INTEREST

Authors approve that to the best of their knowledge, there is not any conflict of interest or common interest with an institution/organization or a person that may affect the review process of the paper.

REFERENCES

1. S. Kim, C. Laschi and B. Trimmer. Soft robotics: A bioinspired evolution in robotics. Trends in Biotechnology 4, 5 (2013) 287-294.
2. C. Laschi and B. Mazzolai. Lessons from animals and plants: The symbiosis of morphological computation and soft robotics. IEEE Robotics & Automation Magazine 23, 3 (2016) 107-114.
3. M. S. Xavier, A. J. Fleming and Y. K. Yong. Experimental characterisation of hydraulic fiber-reinforced soft actuators for worm-like robots. Paper presented at 7th International Conference on Control, Mechatronics and Automation, TU Delft, Netherlands, 6-8 November. pp. 204-209, 2019.
4. Jin, T., Sun, Z., Li, L. et al. Triboelectric nanogenerator sensors for soft robotics aiming at digital twin applications. Nature Communucations 11, 5381 (2020).
5. P. Ferrentino, K. T. Seyedreza, J. Brancart, G. Van Assche, B. Vanderborght and S. Terryn. FEA-Based Inverse Kinematic Control: Hyperelastic Material Characterization of Self-Healing Soft Robots in IEEE Robotics & Automation Magazine (2021) 2-12.
6. A. L. Gunderman, J. A. Collins, A. L. Myers, R. T. Threlfall and Y. Chen, Tendon-Driven Soft Robotic Gripper for Blackberry Harvesting. IEEE Robotics and Automation Letters 7, 2 (2022) 2652-2659.
7. X. Huang, K. Kumar, M. Khalid Jawed, Z. Ye and C. Majidi. Soft Electrically Actuated Quadruped (SEAQ)—Integrating a Flex Circuit Board and Elastomeric Limbs for Versatile Mobility. IEEE Robotics and Automation Letters 4, 3 (2019) 2415-2422.
8. M. A. İ. Kalın, C. Aygül, A. Türkmen, J. Kwiczak-Yiğitbaşı, B. Baytekin and O. Özcan. Design, Fabrication, and Locomotion Analysis of an Untethered Miniature Soft Quadruped, SQuad. IEEE Robotics and Automation Letters 5, 3 (2020) 3854-3860.
9. D. Özbek, T. B. Yılmaz, M. A. İ. Kalın, K. Şentürk and O. Özcan. Detecting Scalable Obstacles Using Soft Sensors in the Body of a Compliant Quadruped. IEEE Robotics and Automation Letters 7, 2 (2022) 1745-1751.
10. Wehner, M., Truby, R., Fitzgerald, D. et al. An integrated design and fabrication strategy for entirely soft, autonomous robots. Nature 536 (2016) 451–455.
11. T. G. Thuruthel, B. Shih, C. Laschi and M. T. Tolley. Soft robot perception using embedded soft sensors and recurrent neural networks. Science Robotics 4, 26 (2019) eaav1488.
12. B. Shih et al. Design considerations for 3D printed soft multimaterial resistive sensors for soft robotics. Frontiers in Robotics and AI 6 (2019).
13. K. B. Justus et al. A biosensing soft robot: Autonomous parsing of chemical signals through integrated organic and inorganic interfaces. Science Robotics 4, 31 (2019) eaax0765.
14. A. Atalay et al. Batch fabrication of customizable silicone-textile composite capacitive strain sensors for human motion tracking. Advance Materials Technologies 2, 9 (2017) 1700136.
15. Y. Mengüç et al. Wearable soft sensing suit for human gait measurement. The International Journal of Robotics Research 33, 14 (2014) 1748-1764.
16. GONG, Jun, et al. MetaSense: Integrating Sensing Capabilities into Mechanical Metamaterial. Paper presented at The 34th Annual ACM Symposium on User Interface Software and Technology, Virtual Event USA, 10-14 October. E-Publishing Inc., New York, pp. 1063–1073, 2021.
17. W.-Y. Li, A. Takata, H. Nabae, G. Endo and K. Suzumori. Shape recognition of a tensegrity with soft sensor threads and artificial muscles using a recurrent neural network. IEEE Robotics and Automation Letters 6, 4 (2021) 6228-6234.
18. TAWK, Charbel, et al. Soft pneumatic sensing chambers for generic and interactive human–machine interfaces. Advanced Intelligent Systems 1,1 (2019) 1900002.
19. C. To, T. L. Hellebrekers and Y. -L. Park. Highly stretchable optical sensors for pressure, strain, and curvature measurement. Paper presented at IEEE/RSJ International Conference on Intelligent Robots and Systems, 28 September - 2 October. pp. 5898-5903, 2015.
20. Jones, R.M. Mechanics of Composite Materials, second ed. CRC Press, Boca Raton, 1999.